Proceeding of the IEEE
International Conference on Robotics and Biomimetics
Dali, China, December 2019

# Leg Spring Parameters Design for a Six-Legged Walking Robot

Huayang Li, Chenkun Qi
*School of Mechanical Engineering*
*Shanghai Jiao Tong University*
*Shanghai, China*
chenkqi@sjtu.edu.cn

Yan Xing, Yong Hu
*Science and Technology on Space Intelligent Laboratory*
*Beijing Institute of Control Engineering*
*Beijing, China*
13717990916@163.com

Feng Gao
*School of Mechanical Engineering*
*Shanghai Jiao Tong University*
*Shanghai, China*
fengg@sjtu.edu.cn

***Abstract* - This paper studies the leg spring parameters design problem for the modular leg mechanism of a six-legged walking robot. The performance metrics and design concept of the six-legged walking robot are proposed primarily. The modular planar leg mechanism with two degrees of freedom is designed based on the pantograph mechanism, and parameters are determined by the workspace analysis considering the walking speed and the maximum step barrier height. Parallel spring is configured on the leg mechanism to reduce the peak output joint torque, and the optimal spring parameters are derived by the proposed method. The effectiveness of the leg spring design method is then verified by simulations carried out with different spring stiffness.**

***Index Terms* - *leg mechanism, mechanism design, spring design, six-legged robot, walking robot***

## I. Introduction

Elasticity is an essential property of legged locomotion of animals. The two primary ways of implementing elastic components in the leg mechanism of walking robots are to place springs in parallel or in series with the actuator [1].

Springs mounted to the leg mechanisms are capable of compensating for the mechanical impact of the collision with the ground in the unconstructed environment. Series elasticity is passively configured along the shank in the leg mechanism to mitigate the impact, such as the Bigdog [2], Scalf [3], HyQ [4], and Hytro-II [5]. Mechanisms with the application of springs are also evaluated to save energy in walking and running [6]. Elastically suspended loads can decrease the energetic cost of legged robot locomotion compared with rigidly attached loads [7]. Parallel springs configured in the leg mechanism can reduce the maximum cylinder force to save the energy of the hydraulically actuated legged robot [8]. Self-stability and robot speed indicated by the Froude number can be significantly improved by adding distal in-series elasticity [9]. Series elasticity produced by a torsion spring mounted into the actuator can elevate the lift-off velocity as well as the jumping height [10]. The robot SpaceBok implements parallel elasticity in the leg mechanism to recuperate energy during jumping and explore continuous jumping gait in the low gravity environment [11]. The jumping robot Grillo implements passive, compliant forelegs to cushion the ground impact, and serially configured springs actuated by a click mechanism in the rear legs to increase the jumping height [12]. The legged robot with wheeled morphology, such as R2-SLIP [13], Edubot [14], and RHex [15], incorporates variable stiffness legs to improve locomotion performance. Compliance applied in parallel manipulators can significantly reduce the actuator effort within a range of desired operating conditions [16].

The rest of the paper is organized as follows. In section II, the design concept of a six-legged walking robot is presented. In section III, the leg mechanism design is discussed. In section IV, the spring parameters design is introduced. In section V, the effectiveness of the leg spring design is verified.

## II. The Six-Legged Walking Robot

### A. Performance Metrics

In this paper, a six-legged walking robot is designed to traverse at a minimum velocity of $0.5\mathrm{km/h}$ with the gait cycle $\mathrm{T} = 1\mathrm{s}$. The robot is also capable of surmounting vertical obstacle with a maximum height of $300\mathrm{mm}$ and climbing the steep slope no less than 30 degrees.

### B. Design Concept

The prototype of the six-legged walking robot is composed of a hexagonal torso and six modular leg mechanisms, as shown in Fig. 1. Each leg mechanism can be regarded as an active suspension system when traversing on irregular terrains.

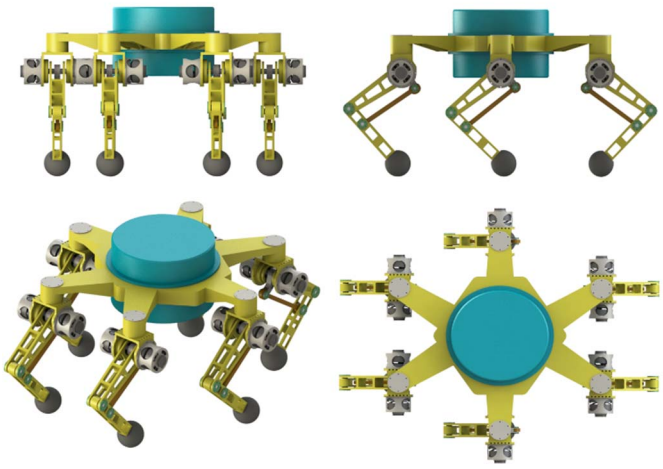

Fig. 1. The prototype of the six-legged walking robot

To maximize the physical performance, high stiffness but lightweight materials such as aluminum alloy and carbon fiber are employed to fabricate the mechanical elements. Electrical motors with a high power-to-weight ratio drive all the active joints. The parallel spring of the leg mechanism is designed in

978-1-7281-6321-5/19//$31.00 ©2019 IEEE

order to reduce the peak driving torque of the motors, which will be discussed in section IV.

## II. The Modular Leg Mechanism

### A. Leg Mechanism

As shown in Fig. 2, the leg mechanism is derived from the pantograph mechanism which has been widely used in the design of walking robots [17] [18]. The two actuators of the leg mechanism are coaxially mounted on the base to minimize the leg inertia. The thigh is directly actuated, while the shank is actuated by a couple of connecting rods labeled as AB and BD.

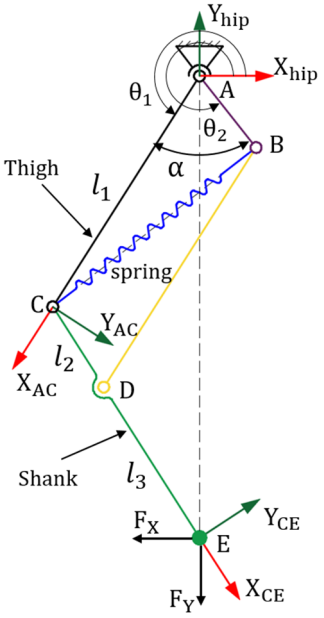


Fig. 2. Schematic diagram of the leg mechanism

### B. Kinematics Model

Fig. 2 presents the schematic kinematic model parameters and coordinate systems of the leg mechanism. The forward kinematics concerning the hip coordinate system can be derived as follows

$$\begin{cases} x = l_1 c_1 + (l_2 + l_3) c_2 \\ y = l_1 s_1 + (l_2 + l_3) s_2 \end{cases} \tag{1}$$

where $[x, y]^T$ denotes the position of point E of the foot relative to the hip coordinate. $l_1$ denotes the length of the thigh AC, $l_2$ and $l_3$ denote the length of the two parts of the shank. $s_1$ and $c_1$ denote the sine function and cosine function of $\theta_1$, $s_2$ and $c_2$ denote the sine function and cosine function of $\theta_2$.

Within the single-leg workspace, the joint angle $[\theta_1, \theta_2]^T$ can be calculated analytically when the desired leg trajectory $[x, y]^T$ concerning the hip coordinate system is prescribed, as shown in (2), (3), and (4).

$$\theta_1 = atan2(y, x) - acos\left(\frac{x^2+y^2+l_1^2-(l_2+l_3)^2}{2l_1\sqrt{x^2+y^2}}\right) \tag{2}$$

$$\theta_2 = \theta_1 + \alpha \tag{3}$$

where

$$\alpha = acos\left(\frac{x^2+y^2-l_1^2-(l_2+l_3)^2}{2l_1(l_2+l_3)}\right) \tag{4}$$

Note that $\alpha$ should always be positive due to the structurally limited motion range.

The forward kinematics concerning the hip coordinate system can be derived in (5) by differentiating (1)

$$\begin{bmatrix} \dot{x} \\ \dot{y} \end{bmatrix} = \begin{bmatrix} -l_1 s_1 & -(l_2 + l_3) s_2 \\ l_1 c_1 & (l_2 + l_3) c_2 \end{bmatrix} \begin{bmatrix} \dot{\theta}_1 \\ \dot{\theta}_2 \end{bmatrix} \tag{5}$$

The static Jacobian matrix can be derived by virtual work principle without taking the mounted spring into account.

$$\begin{bmatrix} \tau_1 \\ \tau_2 \end{bmatrix} = \begin{bmatrix} -l_1 s_1 & l_1 c_1 \\ -(l_2 + l_3) s_2 & (l_2 + l_3) c_2 \end{bmatrix} \begin{bmatrix} F_x \\ F_y \end{bmatrix} \tag{6}$$

where $F_x$ and $F_y$ denote the output force of the foot tip along the X-axis and Y-axis with $\tau_1$ and $\tau_2$ determined.

### C. Workspace Analysis

As shown in Fig. 3, the motion range of the driving joint can be expressed as

$$\pi - \varphi \le \theta_1 \le \theta_2 \le 2\pi + \varphi \tag{7}$$

where $\varphi$ is a structure parameter that depends on the interference of thigh $AC$ and motor base. Considering the motion range of the joint, the reachable region of the foot tip can be theoretically determined by the parameter $l_1$, $l_2$, $l_3$ and $\varphi$. To increase the single-leg workspace, $\varphi$ should be made as large as possible. The shape of the leg workspace varies with variable $p$, where $p$ is defined as follows

$$p = \frac{l_2 + l_3}{l_1} \tag{8}$$

It can be proved that the workspace is symmetric about $Y_{hip}$ axis only if $p = 1$. In order to make the leg ability identical in the forward and backward direction, the rest of the paper will be carried out with the assumption that $p = 1$. Singular positions are the lower outer boundary of the workspace, which is indicated by the light green dotted line.

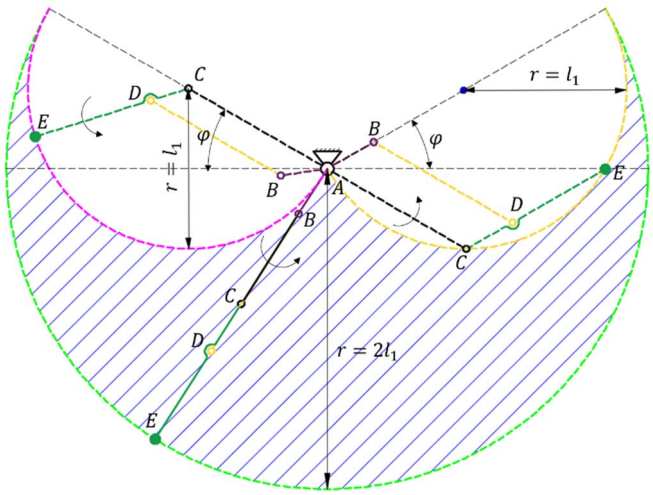


Fig. 3. Schematic diagram of the single-leg workspace when $p = 1$

### D. Determination of Leg Mechanism Parameters

As shown in Fig. 4, the single-leg workspace should satisfy the requirements of minimum step length as well as the height of the step barrier. Walking speed as well as the ability to surmount irregular terrains can be significantly enhanced with the increase of the parameter $l_1$, while the required joint torque $\tau_1$ and $\tau_2$ will also increase, according to the equation (6). To make the overall structure of the six-legged walking robot compact, the parameter $l_1$ should be set as small as possible on the premise of satisfying the abilities mentioned above.

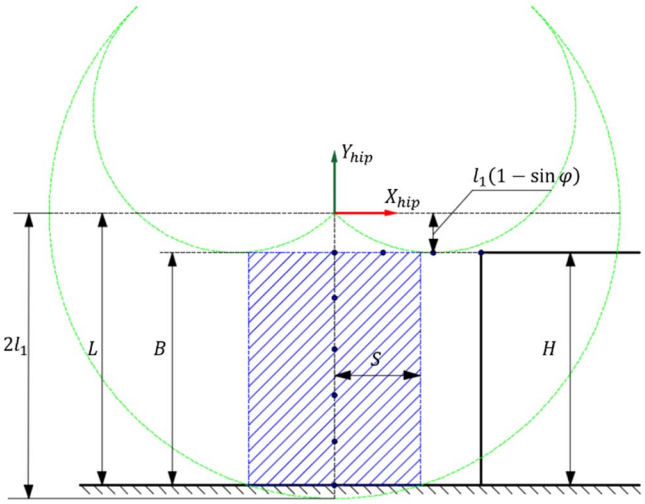


Fig. 4. Single-leg workspace with step barrier

The average walking speed can be calculated as

$$v = \frac{S}{\beta T} \tag{9}$$

where $S$ is the step length, $\beta$ is the duty factor, and $T$ is the time of a gait cycle.

The lower boundary of the single-leg workspace satisfies the following equation

$$x^2 + y^2 = 4{l_1}^2 \tag{10}$$

Parameters of the sing-leg workspace should meet the following constraints to surmount the step barrier with the height of $H$

$$B \geq H \tag{11}$$

where

$$B = L - (1 - \sin\varphi) l_1 \tag{12}$$

$$L = \sqrt{4{l_1}^2 - S^2} \tag{13}$$

Substitute (12) and (13) into (11), $l_1$ can be calculated as

$$l_1 = \frac{2aH + \sqrt{(2aH)^2 + 4(4-a^2)(S^2+H^2)}}{2(4-a^2)} + \sigma \tag{14}$$

where $\sigma$ is the compensation for the interference among the mechanism. To reduce the inertia, parameter $l_1$ should be set as small as possible under the condition of terrain traversing. Finally, the parameter $l_1$ is set as $250\text{mm}$.

## IV. The Spring Parameters Design

### A. Torque Distribution in the Workspace

As shown in Fig. 5, the torque distribution of the two driving joints in the single-leg workspace can be divided into three subspaces. In subspace 1, $\tau_1 > 0, \tau_2 > 0$, in subspace 2, $\tau_1 > 0, \tau_2 < 0$ and in subspace 3, $\tau_1 < 0, \tau_2 < 0$. Locations of the three subspaces will vary with a variable $q$

$$q = \frac{F_x}{F_y} \tag{15}$$

which can be calculated by the maximum robot acceleration. Taking $q = -0.2$ as an example, in this case, the robot is in the deceleration stage with acceleration $\text{a} = 0.2\text{g}$

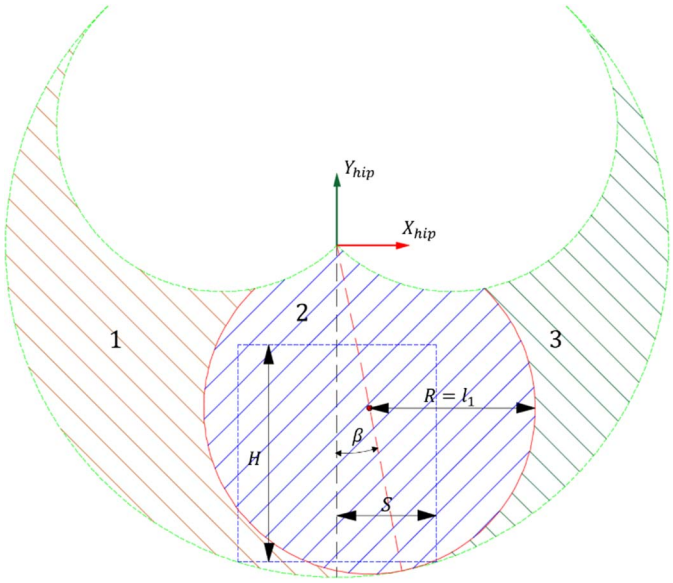


Fig. 5. Torque distribution in the single-leg workspace

The boundary of subspace 2 can be expressed as

$$(x - l_1\cos\beta)^2 + (y - l_1\sin\beta)^2 = {l_1}^2 \tag{16}$$

where

$$\beta = atan2(F_y, F_x) + 2\pi, F_y < 0 \tag{17}$$

The design of the spring parameter will be based on the torque distribution in subspace 2 because the leg trajectory is enclosed in it at almost all times even in the acceleration and deceleration stage when $q$ is not equal to zero. It can be drawn that the peak value of $\tau_1$ is positive and the peak value of $\tau_2$ is negative.

*B. Spring Configuration*

As illustrated in Fig. 2, a parallel spring mounted between point B and point C is employed because serial elastic springs cannot reduce the maximum output torque of the actuators.

When taking the mounted spring into account, the static Jacobian matrix can be derived as follows

$$\begin{bmatrix}\tau_1'\\ \tau_2'\end{bmatrix} = l_1\begin{bmatrix}-s_1 & c_1\\ -s_2 & c_2\end{bmatrix}\begin{bmatrix}F_x\\ F_y\end{bmatrix} - \begin{bmatrix}L_1\\ L_2\end{bmatrix} \tag{18}$$

where

$$L_1 = kl_1l_2\left(1-\frac{l_{ini}}{l_{spr}}\right)\sin(\alpha) \tag{19}$$

$$L_2 = -L_1 \tag{20}$$

$l_{ini}$ is the initial length of the spring, $\alpha = \theta_2 - \theta_1$, $l_{spr}$ is the spring length

$$l_{spr} = \left({l_1}^2 + {l_2}^2 - 2l_1l_2\cos(\alpha)\right)^{\frac{1}{2}} \tag{21}$$

at a specific configuration when $\theta_1$ and $\theta_2$ are determined.

To reduce the peak joint torque, the corresponding value of $L_1$ should be positive and the value of $L_2$ should be negative when $\tau_1$ and $\tau_2$ reach the peak value separately. As shown in Fig. 6, the initial length of the spring, as well as the spring property (stretched spring or compressed spring), can affect the reachable workspace as well as the value of $L_1$ and $L_2$.

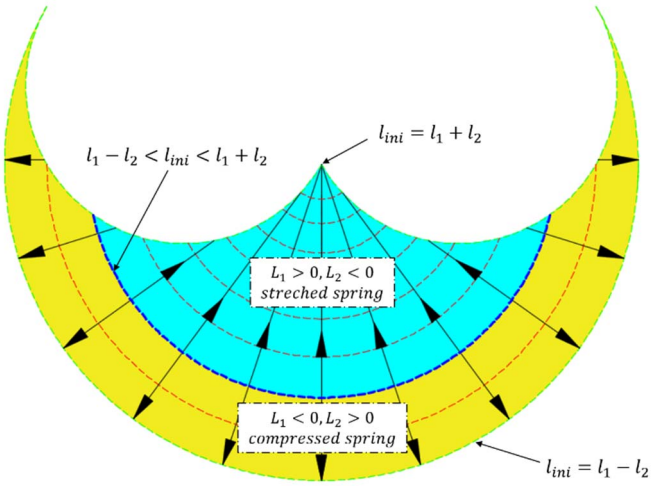


Fig. 6. Influence of the spring's initial length and property

When $l_1 - l_2 < l_{ini} < l_1 + l_2$, the entire workspace is divided into the blue part (in which $L_1 > 0$) and the yellow part (in which $L_1 < 0$). If a stretched spring is mounted to the mechanism, then the yellow part will be unreachable, while if a compressed spring is mounted to the mechanism, then the blue part will be unreachable. The greater the initial length of the spring, the greater the area of the yellow part. When $l_{ini} = l_1 + l_2$, the yellow part covers the entire workspace; when $l_{ini} = l_1 - l_2$, the blue part covers the entire workspace.

Subspace 2 is the most frequently used area of the single-leg workspace in which $\tau_1 > 0$ and $\tau_2 < 0$. So a stretched spring with the initial length $l_{ini} = l_1 - l_2$ is employed to maximize the reachable workspace as well as reduce the output torque of joint 1 and joint 2. Because this configuration can ensure that $L_1 > 0$ and $L_2 < 0$ in subspace 2.

*C. Energy Expenditure due to Spring Installation*

Energy expenditure of joints without spring mounted to the mechanism can be calculated as

$$W = \int \tau_1\, d\theta_1 + \int \tau_2\, d\theta_2 \tag{22}$$

Energy expenditure of joints with spring mounted to the mechanism can be calculated as

$$W' = \int \tau_1'\, d\theta_1 + \int \tau_2'\, d\theta_2 \tag{23}$$

Subtract (22) with (23), the variation of the energy expenditure can be expressed as

$$W_s = \int(\tau_1 - \tau_1')\, d\theta_1 + \int(\tau_2 - \tau_2')\, d\theta_2 \tag{24}$$

Substitute (6) and (18) into (24), $W_s$ can be expressed as

$$W_s = \int(L_1 d\theta_1 + L_2 d\theta_2) \tag{25}$$

Substitute (20) into (25), $W_s$ can be expressed as

$$W_s = \int -L_1 d\alpha \tag{26}$$

Substitute (19) into (26), $W_s$ can be calculated as

$$W_s = \left(kl_1l_2\cos(\alpha) + kl_{ini}l_{spr}\right)\Big|_{\alpha_j}^{\alpha_i} \tag{27}$$

As shown in Fig. 7, $\alpha_i (1 \le i \le 4)$ is the corresponding value of $\alpha$ when the foot end is located at the initial position, $\alpha_j (1 \le j \le 4)$ is the corresponding value of $\alpha$ when the foot end is located at the final position.

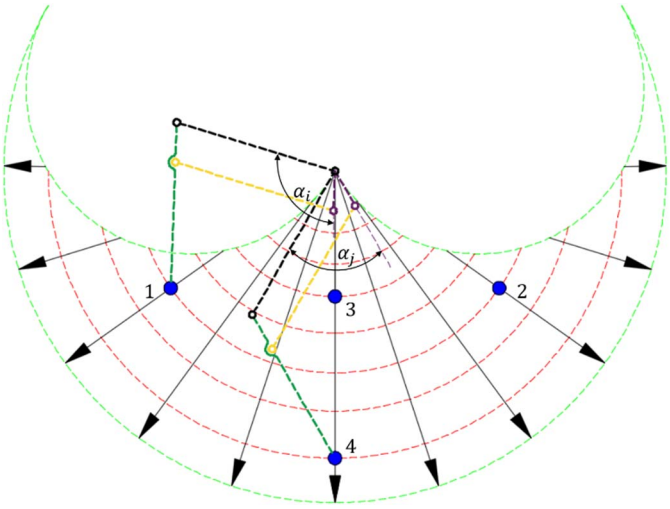


Fig. 7. Distribution of energy expenditure in the workspace

The directions indicated by the solid black arrows represent the descendant directions of the energy expenditure. When the foot tip moves along a particular arc, e.g., arc 1-2, the spring does not affect the energy expenditure of the system. When the foot tip is located in an arc along the positive directions relative to the initial position, e.g., arc 3-4, the energy expenditure of the system will be reduced. When the end position of the foot

tip is located in an arc along the negative directions relative to the initial position, e.g., arc 4-3, the energy expenditure of the system will be increased.

### D. Influence of Mechanism Parameters

To explore the relationship between parameter $r$ and $L_1$, an evaluation index is defined as $F_l$ which have no concern with the spring stiffness $k$.

$$F_l = \frac{L_1}{k} = r{l_1}^2\left(1 - \frac{l_{ini}}{l_1\sqrt{1+r^2-2r\cos(\alpha)}}\right)\sin(\alpha) \tag{28}$$

where

$$r = l_2/l_1 \tag{29}$$

Let the derivative of $F_l$ be zero, the arithmetic solution ω associated with $r$ can be derived. When the foot end position is located at the curve expressed in (30)

$$x^2 + y^2 = 2{l_1}^2(1+\omega) \tag{30}$$

$F_l$ reaches its maximum.

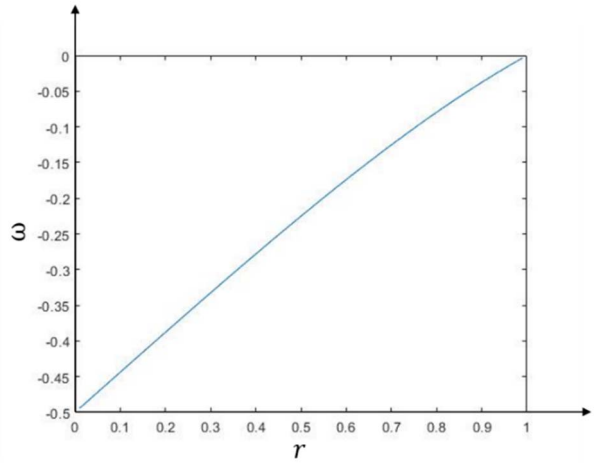


Fig. 8. Relationship between ω and $r$

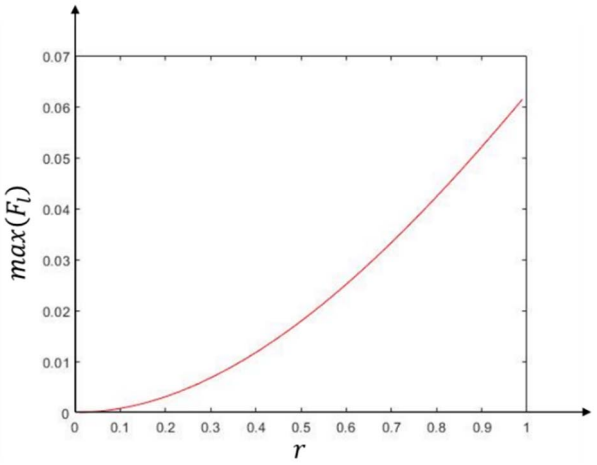


Fig. 9. Relationship between $max(F_l)$ and $r$

As shown in Fig. 8, ω increases with $r$, and the peak position approaches the lower boundary of the workspace in this condition according to (30). In Fig. 9, the maximum value of $F_l$ also increases with $r$. To make the leg mechanism compact, the parameter $r$ is set as 0.4, that is, $l_2 = 100\text{mm}$. Under this condition, $\omega$ equals $-0.2782$, and the maximum value of $F_l$ equals 0.0118. It means that when a spring with the stiffness of $1000\text{N/m}$ is mounted to the leg mechanism, the maximum capability of reducing joint torque is $11.8\text{Nm}$. Trajectory planning of the foot tip will be near the curve mentioned in (30) to minimize the output torque of the two driving joints to the full extent.

### E. Determination of the Spring Stiffness

To reduce the peak torque of joint 1 and joint 2 to the full extent, the following equality constraints should be satisfied separately

$$\tau_{1max} - L_{1a}(k_1) = -\left(\tau_{1min} - L_{1b}(k_1)\right) \tag{31}$$

$$\tau_{2max} - L_{2a}(k_2) = -\left(\tau_{2min} - L_{2b}(k_2)\right) \tag{32}$$

where $L_{1a}(k_1)$ is the corresponding value of $L_1$ when $\tau_1$ reaches the maximum, $L_{1b}(k_1)$ is the corresponding value of $L_1$ when $\tau_1$ reaches the minimum, $L_{2a}(k_2)$ is the corresponding value of $L_2$ when $\tau_2$ reaches the maximum, $L_{2b}(k_2)$ is the corresponding value of $L_2$ when $\tau_2$ reaches the minimum. To reduce the output torque of joint 1 and joint 2 simultaneously, the spring stiffness $k$ can be obtained by the following equation

$$0 \le k \le min(k_1, k_2) \tag{33}$$

## V. Simulation Validation

Walking with the gait cycle of 1s and the step length of 150mm is taken as an example. Based on the above-mentioned method, the initial length of 150mm and the stiffness of $2306\text{N/m}$ are the ideal spring parameters. The simulations with the same initial length and different stiffness are carried out to verify the validity of the leg spring design method.

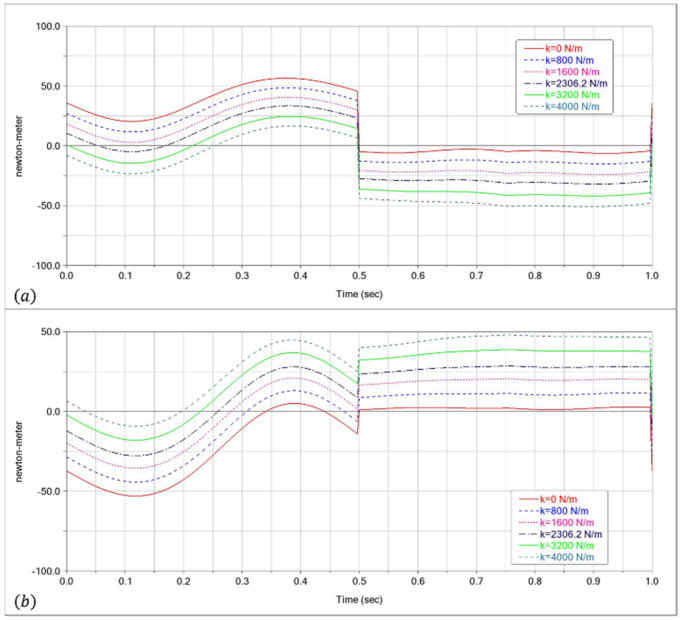


Fig. 10. Torque curves of the driving joints

Fig. 10 (a) presents the output torque curves of joint 1 with springs of different stiffness. Fig. 10 (b) presents the output torque curves of joint 2 with springs of different stiffness. The effectiveness of different stiffness is summarized in Table I. It can be drawn that spring parameters derived from the above-mentioned design method are the ideal parameters to reduce the torque of the driving joints.

TABLE I
EFFECTIVENESS OF DIFFERENT SPRING STIFFNESS

| $k$ | Max. $\mathrm{abs}(\tau_1)$ | $\tau_1$ Reduction (%) | Max. $\mathrm{abs}(\tau_2)$ | $\tau_2$ Reduction (%) |
|---|---|---|---|---|
| 0 N/m | 56.504 Nm | / | 53.026 Nm | / |
| 800 N/m | 48.517 Nm | 14.13 | 44.271 Nm | 16.51 |
| 1600 N/m | 40.534 Nm | 28.26 | 35.515 Nm | 33.02 |
| 2306 N/m | 33.496 Nm | 40.72 | 28.578 Nm | 46.11 |
| 3200 N/m | 41.933 Nm | 25.79 | 38.827 Nm | 26.78 |
| 4000 N/m | 50.897 Nm | 9.92 | 48.001 Nm | 9.48 |

## VI. CONCLUSION

In this paper, parameters of the planar leg mechanism are determined primarily by the requirements of minimum step length as well as the height of the step barrier. Then the leg spring design method for a six-legged walking robot is studied to reduce the required motor peak torque of the driving joints. A series of simulations with different spring stiffness is carried out to verify the effectiveness of the leg spring design method and the resulting torque curves of $\tau_1$ and $\tau_2$ are recorded. When choosing the optimal spring stiffness derived by the above-mentioned design method, the peak joint torque of $\tau_1$ can be reduced by 40.72% and the peak joint torque of $\tau_2$ can be reduced by 46.11%.

## ACKNOWLEDGMENT

This work was funded by the Manned Space Advanced Research Project (Grant No. 030601), and the National Key Research and Development Plan of China (Grant No. 2017YFE0112200).

## REFERENCES

[1] Y. Yesilevskiy, Z. Y. Gan, and C. D. Remy, "Energy-Optimal Hopping in Parallel and Series Elastic One-Dimensional Monopeds," *J. Mech. Robot.*, vol. 10, no. 3, Jun 2018.

[2] D. V. Lee and A. A. Biewener, "BigDog-Inspired Studies in the Locomotion of Goats and Dogs," *Integr. Comp. Biol.*, vol. 51, no. 1, pp. 190-202, Jul 2011.

[3] X. W. Rong, Y. B. Li, J. H. Ruan, and B. Li, "Design and simulation for a hydraulic actuated quadruped robot," *J. Mech. Sci. Technol.,* vol. 26, no. 4, pp. 1171-1177, Apr 2012.

[4] C. Semini, N. G. Tsagarakis, E. Guglielmino, M. Focchi, F. Cannella, and D. G. Caldwell, "Design of HyQ - a hydraulically and electrically actuated quadruped robot," *Proc. Inst. Mech. Eng. Part I-J Sys Control Eng.*, vol. 225, no. I6, pp. 831-849, Sep 2011.

[5] D. P. Lu, E. B. Dong, C. S. Liu, Z. R. Wang, X. G. Zhang, M. Xu, and J. Yang, "Mechanical System and Stable Gait Transformation of a Leg-Wheel Hybrid Transformable Robot," *IEEE/ASME Int. Conf. Adv*, 2013, pp. 530-535.

[6] R. M. Alexander, "Energy-saving mechanisms in walking and running," *J. Exp. Biol.* , vol. 160, pp. 55-69, 1991.

[7] J. Ackerman and J. Seipel, "Energy Efficiency of Legged Robot Locomotion With Elastically Suspended Loads," *IEEE Trans. Robot.*, Article vol. 29, no. 2, pp. 321-330, Apr 2013.

[8] X. B. Chen, F. Gao, C. K. Qi, X. H. Tian, and J. Q. Zhang, "Spring Parameters Design for the New Hydraulic Actuated Quadruped Robot," *J. Mech. Robot.*, vol. 6, no. 2, Jun 2014.

[9] A. Sprowitz, A. Tuleu, M. Vespignani, M. Ajallooeian, E. Badri, and A. J. Ijspeert, "Towards dynamic trot gait locomotion: Design, control, and experiments with Cheetah-cub, a compliant quadruped robot," *Int. J. Robot. Res.*, Article vol. 32, no. 8, pp. 932-950, Jul 2013.

[10] S. Curran, B. T. Knox, J. P. Schmiedeler, and D. E. Orin, "Design of Series-Elastic Actuators for Dynamic Robots With Articulated Legs," *J. Mech. Robot.*, vol. 1, no. 1, Feb 2009.

[11] P. Arm, R. Zenkl, P. Barton, L. Beglinger, A. Dietsche, L. Ferrazzini, "SpaceBok: A Dynamic Legged Robot for Space Exploration," *in Proc. IEEE Int. Conf. Robot. Autom.*, 2019, pp. 6288-6294

[12] U. Scarfogliero, C. Stefanini, and P. Dario, "The use of compliant joints and elastic energy storage in bio-inspired legged robots," *Mech. Mach. Theory.*, vol. 44, no. 3, pp. 580-590, Mar 2009.

[13] K. J. Huang, S. C. Chen, H. Komsuoglu, G. Lopes, J. Clark, and P. C. Lin, "Design and Performance Evaluation of a Bio-Inspired and Single-Motor-Driven Hexapod Robot With Dynamical Gaits," *J. Mech. Robot.*, vol. 7, no. 3, Aug 2015.

[14] K. C. Galloway, J. E. Clark, and D. E. Koditschek, "Variable Stiffness Legs for Robust, Efficient, and Stable Dynamic Running," *J. Mech. Robot.*, vol. 5, no. 1, Feb 2013.

[15] U. Saranli, M. Buehler, and D. E. Koditschek, "RHex: A simple and highly mobile hexapod robot," *Int. J. Robot. Res.*, vol. 20, no. 7, pp. 616-631, Jul 2001.

[16] J. Borras and A. M. Dollar, "Actuation Torque Reduction in Parallel Robots Using Joint Compliance," *J. Mech. Robot.*, vol. 6, no. 2, Jun 2014.

[17] W. Guo, C. R. Cai, M. T. Li, F. S. Zha, P. F. Wang, and K. N. Wang, "A Parallel Actuated Pantograph Leg for High-speed Locomotion," *J. Bionic. Eng.*, Article vol. 14, no. 2, pp. 202-217, Apr 2017.

[18] M. Hutter, C. Gehring, M. A. Hopflinger, M. Blosch, and R. Siegwart, "Toward Combining Speed, Efficiency, Versatility, and Robustness in an Autonomous Quadruped," *IEEE Trans. Robot.*, vol. 30, no. 6, pp. 1427-1440, Dec, 2014.